

# Closed Stream Lines in Uncertain Vector Fields

Mathias Otto \*

Otto-von-Guericke University, Magdeburg

Tobias Germer †

Otto-von-Guericke University, Magdeburg

Holger Theisel ‡

Otto-von-Guericke University, Magdeburg

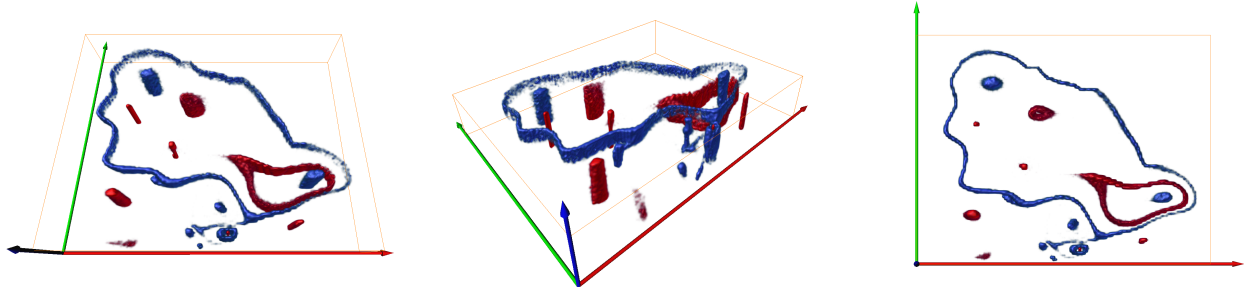


Figure 1: Segment of the Pacific Ocean: volume renderings of the particle distributions visualize attracting (blue) and repelling (red) structures. There are two attracting and two repelling closed stream lines.

## Abstract

We present a method for the detection and visualization of closed stream lines topologically acting as sources or sinks in uncertain 2D and 3D vector fields. For their detection, we apply a Monte Carlo simulation which generates particle distribution functions representing sinks and sources. We show that in the uncertain case there is no structural difference between critical points and closed orbits. This allows the application of critical point extractors to closed stream lines as well. We show applications for some synthetic and real world examples.

**Keywords:** Flow Visualization, Uncertainty, Topology

## 1 Introduction

The representation of uncertainty is one of the most challenging topics in visualization [Johnson 2004]. A lot of approaches have been published for a variety of different data classes. Flow data is a special case, because uncertainty is transported within the flow. Therefore it has to be analyzed globally. To the best of our knowledge, there are only a few publications that treat this topic. In [Otto et al. 2010] a topological analysis of 2D uncertain vector fields is presented that describes the computation and visualization of sink,

source and saddle distributions. In [Otto et al. 2011] this concept was extended for uncertain 3D vector fields. In this work we consider closed stream lines. In vector fields without uncertainty, closed stream lines are topological features that are missing in most topological visualizations of vector field topology, because of their non-local properties. For uncertain vector fields there has been no solution described yet.

In this paper we show that closed stream lines can be found as global features, in particular as sink and source distributions. For this we extend the approaches presented in [Otto et al. 2010] and [Otto et al. 2011] for the detection of closed stream lines. This results in scalar fields, which represent the probability distributions of sinks and sources, respectively. The final visualization is done by volume renderings of these scalar fields. The aim of this paper is the detection of closed orbits, we do not investigate other features like saddles, boundary switches and vortices.

## 2 Related work

The articles [Griethe and Schumann 2006; Johnson and Sanderson 2003; Pang et al. 1997] give an overview of existing uncertainty based visualization approaches. Uncertainty has been considered in different fields of visualization, like isosurface [Djurcilov et al. 2002; Grigoryan and Rheingans 2002; Rhodes et al. 2003; Brown 2004] and information visualization [Streit et al. 2008]. [Maddah et al. 2007; Schultz et al. 2007] proposes probabilistic fiber tracking in DT-MRI visualization. This work relates to our approach but considers different data classes.

Some solutions exist for visualizing local uncertainty. Examples for this kind of visualization are glyphs [Lodha et al. 1996; Wittenbrink et al. 1995], the reaction diffusion model [Sanderson et al. 2004], cross advection and error diffusion [Botchen et al. 2005], and additional color schemes [Botchen et al. 2006]. All of these techniques show the effect of the uncertainty locally or for a very short integration time. They do not show the effect on the global features of the vector field.

\*e-mail: mathias.otto@isg.cs.uni-magdeburg.de

†e-mail: germer@isg.cs.uni-magdeburg.de

‡e-mail: theisel@isg.cs.uni-magdeburg.de

An approach for a global analysis of uncertain vector fields is presented in [Otto et al. 2010]. It is an integration based approach that results in particle density distributions, which represent the probability distributions of sinks and sources. An extension of this approach for uncertain 3D vector fields is presented in [Otto et al. 2011]. The main contribution of this paper is the application of the saddle and boundary switch connectors approaches [Theisel et al. 2003; Weinkauff et al. 2004] to uncertain 3D vector fields. In this paper we will show that based on these two approaches an analysis of attracting and repelling closed orbits in uncertain vector fields can be done.

Closed stream lines in vector fields without considering uncertainty have been considered in [Wischgoll and Scheuermann 2001]. This approach works on 2D vector fields. This approach has been extended to 2D time dependent vector fields [Wischgoll et al. 2001] and to 3D vector fields [Wischgoll and Scheuermann 2002]. These approaches are based on a tracking of streamlines. These methods work on the cells of the data grid by finding cell cycles and analyzing stream lines of their boundary vertices. [Theisel et al. 2004] present a grid-independent approach to 2D closed stream line extraction.

### 3 Uncertain vector field topology

This section reviews the theory of the topology of uncertain 2D vector fields that was presented in [Otto et al. 2010]. For the extraction of closed stream lines we give a definition of uncertain vector fields and concentrate on the extraction of sink and source distributions. Our approach considers only closed stream lines with a sink and source like character. The concepts of the extraction of sinks and sources are directly applicable for 3D uncertain vector fields [Otto et al. 2011].

#### 3.1 Uncertain vector field

An uncertain vector field is generated by multiple measurements or simulations of one flow phenomenon. Instead of assigning a single vector to a point in the domain, a finite number of different vectors characterizes the probabilistic local behavior of a flow. This is interpreted as a probability distribution, which is represented by a 4D scalar field.

**Definition 1** An uncertain 2D vector field in the domain  $\mathbf{D}$  is a 4D scalar field  $\rho_v(x, y; u, v)$  with

- $(x, y) \in \mathbf{D}$  and  $(u, v) \in \mathbb{R}^2$
- $\rho_v(x, y; u, v) \geq 0$
- $\int_{-\infty}^{\infty} \int_{-\infty}^{\infty} \rho_v(x, y; u, v) du dv = 1$ .

The value  $\rho_v(x, y; u, v) du dv$  denotes the probability that at the location  $(x, y)$  the vector field has some value in the range  $[u, u + du] \times [v, v + dv]$ .

#### 3.2 Integration of particle distributions

In contrast to certain vector fields we cannot integrate stream lines in uncertain vector fields. Instead, a particle seeded in such a field will not move to a unique location, because the particle has different probabilities to move to various locations. Therefore, we have to integrate particle distribution functions. For this we define a 2D scalar field  $p(x, y; t)$  that represents the particle distribution, which

will be integrated in an uncertain vector field. This scalar field has to fulfill the following properties:

- $p(x, y; t) \geq 0$  for all  $(x, y) \in \mathbf{D}$  and  $t \geq 0$
- $\int_{\mathbf{D}} p(x, y; t) dx dy \leq 1$  for all  $t \geq 0$ .  
(We use  $\leq$  instead of  $=$  because particles may leave the domain during integration.)

The value  $p(x, y; t) dx dy$  denotes the ratio of particles in  $[x, x + dx] \times [y, y + dy]$  in relation to the initial number of particles in  $\mathbf{D}$  at  $t = 0$ .

To consider the transport of particles in an uncertain vector field  $\rho_v$ , we use the infinite domain  $\mathbf{D} = \mathbb{R}^2$  to avoid boundary effects. The particle distributions are represented by virtual particles without inertia. The particles are transported within a time interval  $\delta t$  that is short enough to assume they are moving on a straight line. At time  $t + \Delta t$  the number of particles in an infinitesimal volume  $dx dy$  at some location  $(x, y)$  is the sum of the numbers of particles in cells  $dr ds$  at all locations  $(r, s)$  times the probabilities that they are transported from  $(r, s)$  to  $(x, y)$  in time  $\Delta t$ , i.e., they experience a velocity  $((x - r)/\Delta t, (y - s)/\Delta t)^T$ . These probabilities are given by  $\rho_v(r, s; \frac{x-r}{\Delta t}, \frac{y-s}{\Delta t}) d(\frac{x-r}{\Delta t}) d(\frac{y-s}{\Delta t})$ . After division by the cell volumes we have  $dx dy = dr ds$ . This yields the following expression for the transport of particle densities:

$$\begin{aligned} p(x, y; t + \Delta t) &= \iint_{\mathbf{D}} p(r, s; t) \rho_v(r, s; \frac{x-r}{\Delta t}, \frac{y-s}{\Delta t}) d(\frac{x-r}{\Delta t}) d(\frac{y-s}{\Delta t}) \\ &= \frac{1}{\Delta t^2} \iint_{\mathbf{D}} p(r, s; t) \rho_v(r, s; \frac{x-r}{\Delta t}, \frac{y-s}{\Delta t}) dr ds \end{aligned}$$

This expression defines a unique integration starting from a given initial particle distribution function.

#### 3.3 Sink and source distributions

For the extraction of sinks and sources we have to start a stream line integration from every point  $(r, s) \in \mathbf{D}$  represented by an initial particle distribution function  $p(x, y; t_0) = \delta(x - r, y - s)$ . In uncertain vector fields, stream lines, sinks, sources and critical points are represented by particle distribution functions. Nevertheless, we still use the terms stream line, sink, source and critical point to refer to these concepts.

**Definition 2** The particle density function  $p_0(x, y)$  is a critical point distribution of  $\rho_v$  if for a stream line integration starting at  $p(x, y; t_0)$  it holds  $\frac{\partial p}{\partial t} = 0$ .

Note that every linear combination of a given number of critical points  $p_1(x, y), \dots, p_n(x, y)$  of  $\rho_v$  is a critical point as well. Formally  $\sum_{i=1}^n \alpha_i p_i$  is a critical point for any  $0 \leq \alpha_1, \dots, \alpha_n \leq 1$  and  $\sum_{i=1}^n \alpha_i \leq 1$ . The sum of all  $\alpha_i$  can be less than one, because particles might leave the domain.

This leads to a continuum of critical points. For the topological analysis we need a set of linearly independent critical points. We call these sets spanning source and sink sequence.

**Definition 3** Given an uncertain vector field  $\rho_v(x, y; u, v)$ , a sequence of sinks  $(p_1(x, y), \dots, p_n(x, y))$  is called spanning sink sequence if  $p_1, \dots, p_n$  are linearly independent and every sink  $p(x, y)$  of  $\rho_v$  can be uniquely described as  $p = \sum_{i=1}^n \alpha_i p_i$  with  $0 \leq \alpha_1, \dots, \alpha_n \leq 1$  and  $\sum_{i=1}^n \alpha_i \leq 1$ . Similarly, a sequence of sources  $(\tilde{p}_1(x, y), \dots, \tilde{p}_m(x, y))$  is called spanning source sequence if  $\tilde{p}_1, \dots, \tilde{p}_m$  are linearly independent and every source  $\tilde{p}(x, y)$  of  $\rho_v$  can be uniquely described as  $\tilde{p} = \sum_{i=1}^m \beta_i \tilde{p}_i$  with  $0 \leq \beta_1, \dots, \beta_m \leq 1$  and  $\sum_{i=1}^m \beta_i \leq 1$ .

### 3.4 Implementation

To implement our approach we employ a Lagrangian Monte-Carlo method. The initial particle density  $p_0$  is represented by a high number of virtual particles without inertia that are advected inside the uncertain vector field. This method is based on probabilistic particle movements. Each particle is integrated by an ‘‘uncertain’’ Euler method. For this a random vector is chosen based on the probabilities that a particle moves from location  $(x, y)$  to any location  $(u, v)$ . These probabilities are stored in the uncertain vector field  $\rho(x, y; u, v)$ . In practice we assume Gaussian distributions to model the uncertainty. Therefore, we have to store only a mean vector field  $v_m(x, y)$  and a tensor field  $T(x, y)$  containing the covariance matrices. In order to speed up the computation, we implemented the integration method in CUDA. In a first step we transfer the uncertain vector field, the particle positions, and for each thread a seed for its random generator into the video memory. Each particle is handled by its own thread. For each particle position the uncertain vector field is trilinearly interpolated resulting in an average vector and a covariance matrix. Then a normally distributed random vector is generated by using a Box-Muller transformation. This random vector is modified by the covariance matrix. Finally we update the particle position by adding the average vector and random vector.

The local rate of change of the particle density is observed over time. For this we count the number of particles inside the cells of a uniform grid. The method terminates if this rate drops under a given threshold. The resulting particle density of the forward integration represents the whole spanning sink sequence and in backward direction the spanning source sequence.

### 3.5 Visualization

Both spanning sink and source sequence are represented by a particle distribution function, that has to be visualized. In order to do that, we use height maps in the 2D case with an underlying LIC of the mean field, as proposed in [Otto et al. 2010]. In the 3D case we choose volume renderings for the visualization of 3D particle distribution functions. These volume renderings are generated with linear transfer functions and specular lighting. In both cases attracting structures are visualized in blue and repelling structures in red.

## 4 Uncertain closed stream lines

In this section we show that the extraction of closed orbits in uncertain vector fields is conceptionally the same as extracting uncertain critical points. To illustrate this, we use two analytic examples for the 2D and 3D case. Then we show that the spanning sink and source sequences contain all closed orbits which act topologically as sink or source.

### 4.1 Synthetic examples

All of our examples assume Gaussian distribution functions in order to model the uncertainty. Each uncertain vector field is represented by a mean vector field and a tensor field containing the covariance matrices.

**Example 1** *The first example illustrates the 2D case. It defines an uncertain vector field over the domain  $\mathbf{D} = [-2, 2] \times [-2, 2]$ . The*

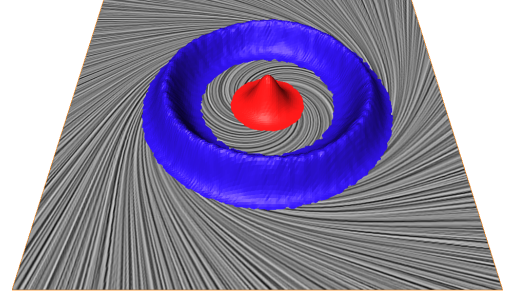


Figure 2: Example 1: attracting closed orbit with a source in the middle

*mean vector field is given as*

$$v_m(x, y) = \begin{bmatrix} y - x \left( \sqrt{x^2 + y^2} - 1 \right) \\ -x - y \left( \sqrt{x^2 + y^2} - 1 \right) \end{bmatrix}$$

*and the covariance matrix as*

$$T(x, y) = \begin{bmatrix} 0.09 & 0 \\ 0 & 0.09 \end{bmatrix}.$$

**Example 2** *In the 3D case we use a similar uncertain vector field where the z-component is added. It is defined over the domain  $\mathbf{D} = [-2, 2] \times [-2, 2] \times [-2, 2]$  with the mean vector field*

$$v_m(x, y, z) = \begin{bmatrix} y - x \left( \sqrt{x^2 + y^2} - 1 \right) \\ -x - y \left( \sqrt{x^2 + y^2} - 1 \right) \\ -z + x \end{bmatrix}$$

*and the covariance matrix*

$$T(x, y, z) = \begin{bmatrix} 0.16 & 0 & 0 \\ 0 & 0.16 & 0 \\ 0 & 0 & 0.16 \end{bmatrix}.$$

### 4.2 Detection

In section 3.3 we showed that sinks and sources of uncertain vector fields are detected by integration of particle distributions until they converge. It turns out that attracting and repelling closed stream lines can be found with this scheme as well. In uncertain vector fields, closed stream lines with attracting and repelling character are also represented by unique critical distributions. These distributions act analogously to ordinary sink or source distributions, because they attract and repel neighboring particles. The main difference is the cyclic movement of particles inside the critical distribution. However, this fluctuation does not influence the shape of the critical distribution, because the particles converge to an asymptotic cyclic distribution. In figure 2 such a particle distribution is shown based on the synthetic example 1.

In order to find such a particle distribution, the integration has to be started at some location that is affected by the closed stream line. The shape of the initial particle distribution is not important. Figure 3 illustrates an integration started from a Delta Dirac function  $p_0 = \delta(1, 0, 0)$ . The integration uses the uncertain vector field defined in example 2. During the first integration steps the particle

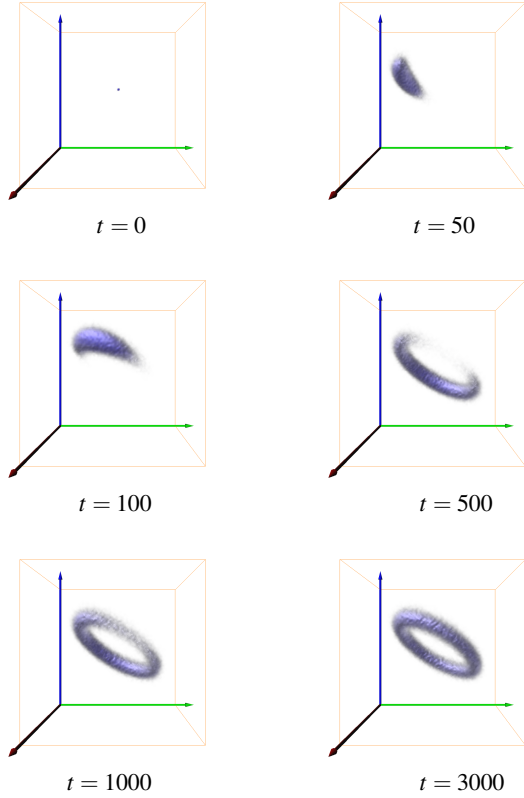


Figure 3: Example 2: volume rendering of the particle density during the integration of one uncertain stream line started at location  $(1, 0, 0)$ .

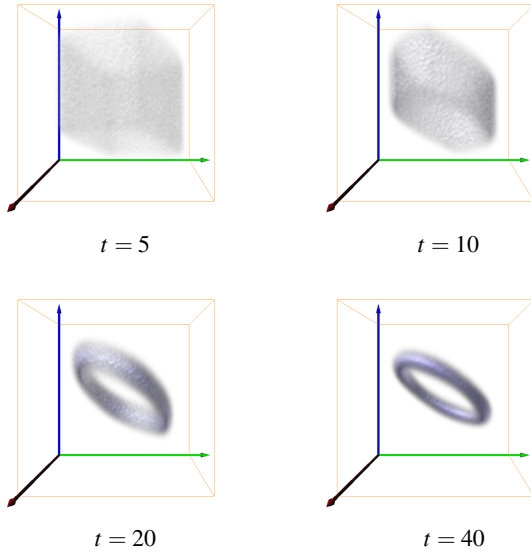


Figure 4: Example 2: volume rendering of the particle density during the integration of one uncertain stream line started from a uniform particle distribution.

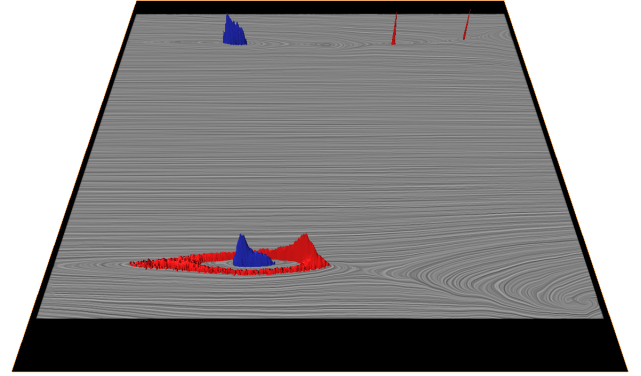


Figure 5: Topology of the uncertain 2D vector fields generated by the PIV measurement of a flow in a tube. Attracting features are visualized in blue, repelling features in red.

distribution moves along the path of the closed orbit. With increasing integration time the particle distribution converges to the distribution of the closed orbit. A faster convergence is achieved by a uniform initial particle distribution as shown in figure 4. The reason for the faster convergence is that the particle distribution does not need to expand from a single point, and the closed orbit acts attracting to all particles in this field. Therefore, they only move to the closed orbit and stay there.

## 5 Results

In this section we demonstrate the detection of closed orbits in uncertain vector fields. We apply our method to some real world examples, like PIV measurements and simulations of oceanic flows, and a synthetic example. All results were created with an Intel Q6600 with 8GB RAM and an Nvidia Geforce 460 GTX with 1 GB VRAM.

### 5.1 Flow in a tube

The first data set is a PIV measurements that consists of 240 snapshots of a slice of a flow in a tube. The measurements are taken from a flow with constant velocity of  $4m/s$ . The timing for the measurements are  $190\mu s$  and the uptake rate  $3,3Hz$ . We used the 240 single 2D velocity fields to generate an uncertain 2D vector field. The uniform data grid has a resolution of  $83 \times 67$ .

Figure 5 shows the resulting uncertain topology. It contains one repelling closed stream line, two sinks and two sources. Figure 6 illustrates the topology of the mean vector field of all 240 measurements, containing five sinks, nine sources and eleven saddles. In comparison the uncertain topology contains less critical structures.

For the computation of the particle distributions representing attracting and repelling structures, we generate a uniform initial distribution with 100 particles per grid cell, with a total of 556100 particles. The computation time for this example is about 25 minutes.

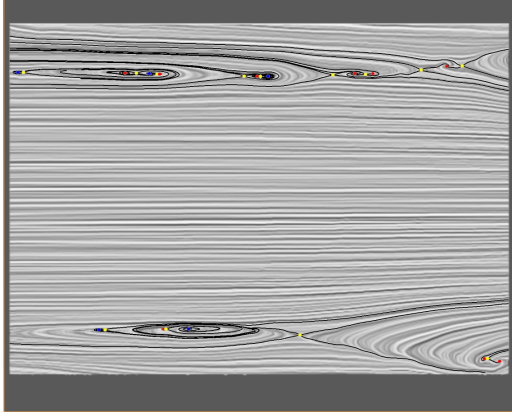


Figure 6: Visualization of topology with underlying LIC of the mean vector field of all PIV measurements. Sinks are blue colored, sources red colored and saddles yellow colored.

## 5.2 Segment of the Pacific Ocean

The second example is based on a flow simulation of the oceans. Here we have got a data set of the global ocean system with average velocity fields of each month over one year. The whole data set has a resolution of  $360 \times 180 \times 40$ . It contains hundreds of critical structures, therefore we picked only a very small segment of the Pacific Ocean in order to show some examples of closed stream lines. The region of interest has a resolution of  $28 \times 22 \times 6$ .

Figure 1 shows some volume renderings of the sink and source distributions of this data set. There are two attracting and two repelling closed stream lines. We adjusted the range of the linear transfer functions to the density of particles on closed stream lines, because there the particles density is much smaller than in the region of real sink and source distributions.

Again, we used a uniform initial particle distribution with 100 particles per grid cell (a total of 369,600 particles). For counting particles in buckets we chose denser grid with a resolution of  $140 \times 110 \times 30$ . The computation time is about 40 minutes.

Furthermore, we use this example to analyze the stability of closed orbits in uncertain vector fields. For this we artificially amplify the uncertainty by factors of 2 and 4. Figure 7 shows results for different amplitudes of uncertainty. The left column shows the critical structures and the right column shows volume renderings of a scalar field  $s$  with

$$s = \frac{\text{maximal Eigenvalue of covariance matrix}}{\text{length of mean vector}}.$$

This gives an impression of the impact of the uncertainty to the movement of particles in the uncertain vector field. For isovalues  $s > 1$  the uncertainty dominates the particle motion. We illustrate this case with an isosurface is shown where  $s = 1$ .

While increasing the uncertainty an attracting closed stream line and a sink distribution become weaker and finally disappear. However repelling structures hardly change, even if they exist in regions where uncertainty dominates, like the the large repelling closed streamline.

To consider the results the stability of critical structures of any type are mainly effected by global uncertainty and not by the the local uncertainty.

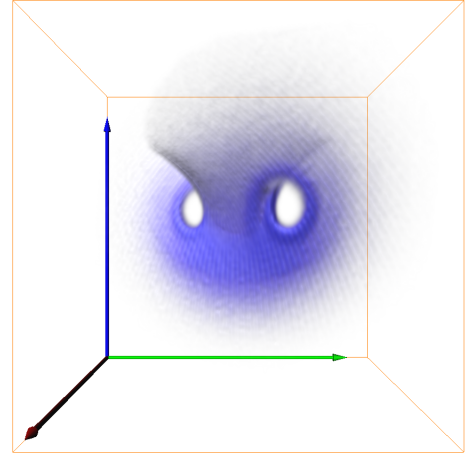


Figure 8: Uncertain Lorenz attractor

## 5.3 Uncertain Lorenz attractor

The last example is derived from the well-known Lorenz attractor, which has no closed stream line in the strict sense. Here we want to show that our method also works for uncertain strange attractors. We set up an uncertain vector field with the Lorenz attractor as mean field:

$$v_m(x, y, z) = \begin{bmatrix} \sigma(y-x) \\ rx - y - xz \\ xy - bz \end{bmatrix}.$$

with

$$T(x, y, z) = \begin{bmatrix} 0.16 & 0 & 0 \\ 0 & 0.16 & 0 \\ 0 & 0 & 0.16 \end{bmatrix}, \quad \sigma = 28, \quad r = 10 \text{ and } b = \frac{8}{3}.$$

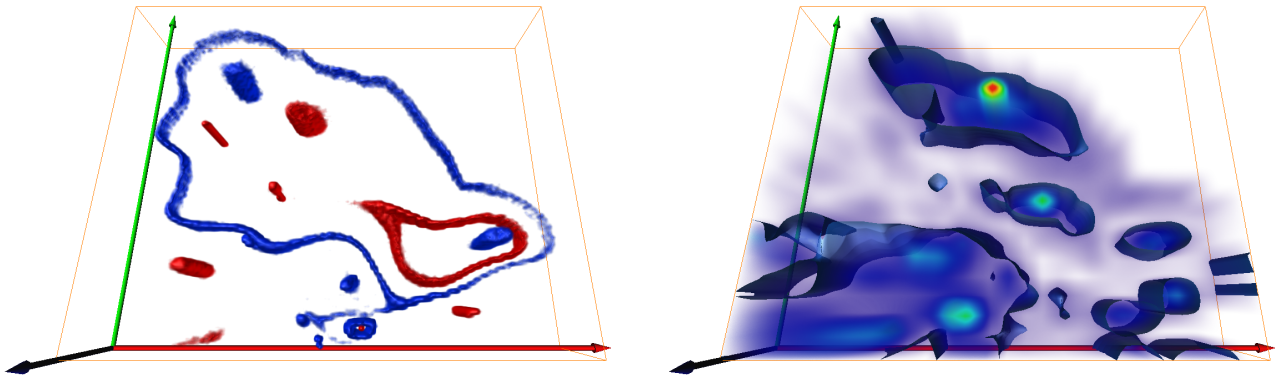
This field is defined over the domain  $\mathbf{D} = [-25, 25] \times [-25, 25] \times [0, 50]$ . Figure 8 shows the critical particle distribution which is created by a forward integration of a uniform initial distribution with 30 particles per grid cell (a total of 3750000 particles). The algorithm converges after 250 integration steps, with a step size of  $\Delta t = 0.02$ . The computation time is 42 seconds. Although the mean field includes a strange attractor instead of a closed stream line, our method still finds this structure.

## 5.4 Computation times

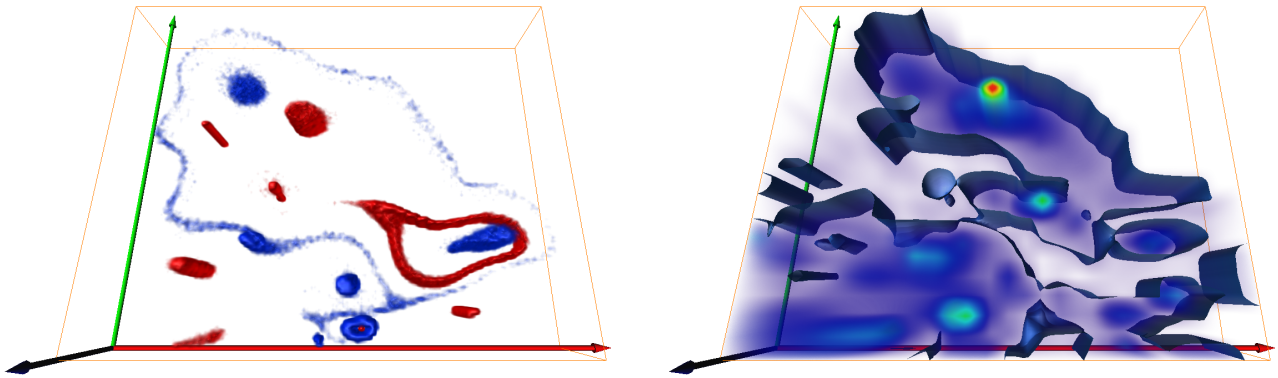
The computation times of the three examples differ significantly. The last example with the highest number of particles and the largest grid is the fastest. The main factor is the uncertain vector field itself. Regions with low velocity and high uncertainty lead to slow convergence and a high number of needed integration steps. Another reason for long run times are strong differences in the velocity field, because the integration step size has to be adapted to the fastest regions in order to detect all features in these regions.

## 6 Conclusion

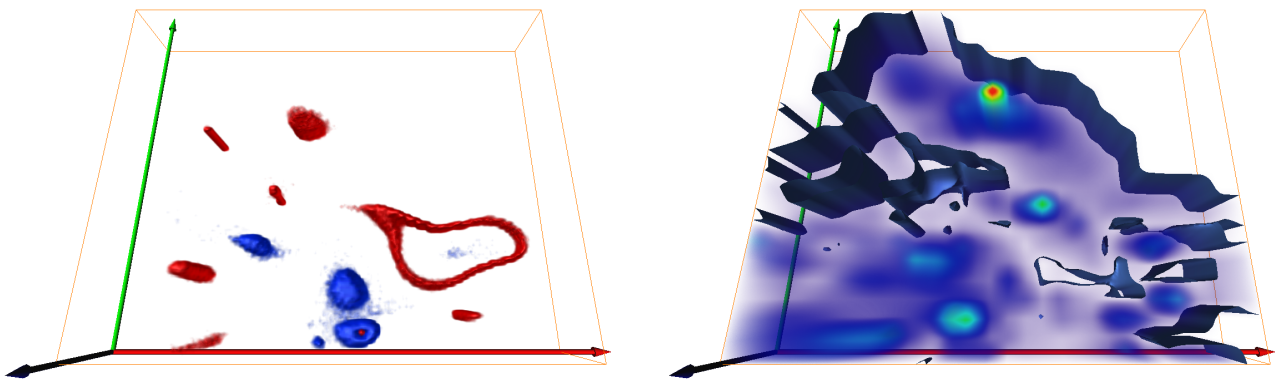
To the best of our knowledge, this is the first approach that considers closed stream lines in the context of uncertain vector fields. In this



1× uncertainty



2× uncertainty



4× uncertainty

Figure 7: Segment of the Pacific Ocean with different amount of uncertainty: (*left column*) Volume renderings of the particle distributions visualize attracting (blue) and repelling (red) structures. While the uncertainty increases, the big attracting closed stream line becomes weaker until it disappears. (*right column*) Volume renderings of a scalar field  $s$  and an isosurface with  $s = 1$ . For the region where  $s > 1$  the uncertainty dominates the particle motion in the uncertain vector field.

paper we have shown that the method proposed in [Otto et al. 2010] can be applied in order to detect closed orbits in uncertain 2D vector fields. We also showed that this method can be extended to detect attracting and repelling closed stream lines in uncertain 3D vector fields. Such attracting and repelling features are the asymptotic result of an uncertain streamline integration represented by particle distributions. We demonstrated the functionality of this method based on several examples. We have also shown that the stability of such features mainly depends on the global uncertainty. Local uncertainty cannot be taken alone to make statements about the stability of critical distributions. Furthermore, we have also shown that other attracting and repelling structures like strange attractors can be detected with this method.

One limitation of our method is that closed stream lines with saddle-like behavior cannot be detected, because these structures are unstable under forward and backward integration. The extraction of such structures will be a topic for future work. Other future goals are the detection of vortex structures of uncertain vector fields, like vortex cores and vortex regions, and the consideration of uncertain unsteady vector fields.

## Acknowledgments

removed for blind submission

We thank Hans-Christian Hege from the ZIB and Martin Hecklau from TU Berlin for providing the PIV data set, and Niklas Röber and Michael Böttinger from DKRZ for the ocean data set.

The pictures were generated using Amira. This work was funded by the Sem-Seg project under the EU FET-Open grant 226042.

## References

- BOTCHEN, R. P., WEISKOPF, D., AND ERTL, T. 2005. Texture-based visualization of uncertainty in flow fields. In *IEEE Visualization*, 647–654.
- BOTCHEN, R. P., WEISKOPF, D., AND ERTL, T. 2006. Interactive Visualization of Uncertainty in Flow Fields using Texture-Based Techniques. In *Proc. Intl. Symp. on Flow Visualization*.
- BROWN, R. 2004. Animated visual vibrations as an uncertainty visualisation technique. In *Proc. GRAPHITE*, 84–89.
- DJURCILOV, S., KIM, K., LERMUSIAUX, P. F. J., AND PANG, A. 2002. Visualizing scalar volumetric data with uncertainty. *Computers and Graphics* 26, 2, 239–248.
- GRIETHE, H., AND SCHUMANN, H. 2006. The visualization of uncertain data: Methods and problems. In *SimVis*, 143–156.
- GRIGORYAN, G., AND RHEINGANS, P. 2002. Probabilistic surfaces: point based primitives to show surface uncertainty. In *IEEE Visualization*, 147–154.
- JOHNSON, C., AND SANDERSON, A. 2003. A next step: Visualizing errors and uncertainty. *IEEE Comput. Graph. Appl.* 23, 5, 6–10.
- JOHNSON, C. 2004. Top scientific visualization research problems. *IEEE Comput. Graph. Appl.* 24, 4, 13–17.
- LODHA, S. K., PANG, A., SHEEHAN, R. E., AND WITTENBRINK, C. M. 1996. Uflow: visualizing uncertainty in fluid flow. In *IEEE Visualization*, 249.
- MADDAH, M., III, W. M. W., WARFIELD, S. K., WESTIN, C.-F., AND GRIMSON, W. E. L. 2007. Probabilistic clustering and quantitative analysis of white matter fiber tracts. In *Proc. IPMI*, vol. 20, 372–383.
- OTTO, M., GERMER, T., HEGE, H.-C., AND THEISEL, H. 2010. Uncertain 2d vector field topology. *Computer Graphics Forum (Proceedings of Eurographics 2010, Norrköpping, Sweden)* 29, 2, 347–356.
- OTTO, M., GERMER, T., AND THEISEL, H. 2011. Uncertain topology of 3d vector fields. In *accepted for 4th IEEE Pacific Visualization Symposium (Proceedings PacificVis 2011)*.
- PANG, A. T., WITTENBRINK, C. M., AND LODHA, S. K. 1997. Approaches to uncertainty visualization. *The Visual Computer* 13, 370–390.
- RHODES, P. J., LARAMEE, R. S., BERGERON, R. D., AND SPARR, T. M. 2003. Uncertainty visualization methods in iso-surface rendering. In *Eurographics*, 83–88.
- SANDERSON, A. R., JOHNSON, C. R., AND KIRBY, R. M. 2004. Display of vector fields using a reaction-diffusion model. In *IEEE Visualization*, 115–122.
- SCHULTZ, T., THEISEL, H., AND SEIDEL, H.-P. 2007. Topological visualization of brain diffusion MRI data. *IEEE TVCG* 13, 6, 1496–1503.
- STREIT, A., PHAM, B., AND BROWN, R. 2008. A spreadsheet approach to facilitate visualization of uncertainty in information. *IEEE TVCG* 14, 1, 61–72.
- THEISEL, H., WEINKAUF, T., HEGE, H.-C., AND SEIDEL, H.-P. 2003. Saddle connectors - an approach to visualizing the topological skeleton of complex 3d vector fields. In *Proc. IEEE Visualization 2003*, 225–232.
- THEISEL, H., WEINKAUF, T., HEGE, H.-C., AND SEIDEL, H.-P. 2004. Grid-independent detection of closed stream lines in 2d vector fields. In *Proc. Vision, Modeling and Visualization (VMV) 2004*, 421–428.
- WEINKAUF, T., THEISEL, H., HEGE, H.-C., AND SEIDEL, H.-P. 2004. *Boundary Switch Connectors for Topological Visualization of Complex 3D Vector Fields*. 183–192.
- WISCHGOLL, T., AND SCHEUERMANN, G. 2001. Detection and visualization of closed streamlines in planar flows. *IEEE Transactions on Visualization and Computer Graphics* 7, 2, 165–172.
- WISCHGOLL, T., AND SCHEUERMANN, G. 2002. Locating closed streamlines in 3d vector fields. In *VISSYM '02: Proceedings of the symposium on Data Visualisation 2002*, Eurographics Association, Aire-la-Ville, Switzerland, Switzerland, 227–ff.
- WISCHGOLL, T., SCHEUERMANN, G., AND HAGEN, H. 2001. Tracking closed streamlines in time-dependent planar flows. In *In Proceedings of the Vision Modeling and Visualization Conference 2001 (VMV 01)*, 447–454.
- WITTENBRINK, C. M., SAXON, E., FURMAN, J. J., PANG, A., AND LODHA, S. 1995. Glyphs for visualizing uncertainty in environmental vector fields. In *IEEE TVCG*, 266–279.